Coexistence of plastic and partially diffusive phases in a helium-methane compound

Coexistence of plastic and partially diffusive phases in a helium-methane compound

Hao Gao,[1] Cong Liu,[1] Andreas Hermann,[2] Richard J. Needs,[3] Chris J. Pickard,[4,5] Hui-Tian Wang,[1] Dingyu Xing,[1] and Jian Sun[1,*]

1 National Laboratory of Solid State Microstructures, School of Physics and Collaborative Innovation Center of Advanced Microstructures, Nanjing University, Nanjing 210093, China

2 Centre for Science at Extreme Conditions and The School of Physics and Astronomy, The University of Edinburgh, Peter Guthrie Tait Road, Edinburgh EH9 3FD, United Kingdom

3 Theory of Condensed Matter Group, Cavendish Laboratory, J J Thomson Avenue, Cambridge CB3 0HE, UK

4 Department of Materials Science & Metallurgy, University of Cambridge, 27 Charles Babbage Road, Cambridge CB3 0FS, UK

5 Advanced Institute for Materials Research, Tohoku University 2-1-1 Katahira, Aoba, Sendai, 980-8577, Japan

Helium and methane are major components of giant icy planets and are abundant in the universe. However, helium is the most inert element in the periodic table and methane is one of the most hydrophobic molecules, thus whether they can react with each other is of fundamental importance. Here, our crystal structure searches and first-principles calculations predict that a He_3CH_4 compound is stable over a wide range of pressures from 55 to 155 GPa and a $HeCH_4$ compound becomes stable around 105 GPa. As nice examples of pure van der Waals crystals, the insertion of helium atoms changes the original packing of pure methane molecules and also largely hinders the polymerization of methane at higher pressures. After analyzing the diffusive properties during the melting of He_3CH_4 at high pressure and high temperature, in addition to a plastic methane phase, we have discovered an unusual phase which exhibits coexistence of diffusive helium and plastic methane. In addition, the range of the diffusive behavior within the helium-methane phase diagram is found to be much narrower compared to that of previously predicted helium-water compounds. This may be due to the weaker van der Waals interactions between methane

molecules compared to those in helium-water compounds, and that the helium-methane compound melts more easily.

INTRODUCTION

Hydrogen and helium are the most abundant elements in the universe and are significant constituents of the planets in our solar system[1]. Superionicity of hydrogen in ice and ammonia was discovered in early works[2–4]. In the superionic state, some atoms form a fixed sublattice while the others diffuse as in a liquid. These states have attracted much interest in planetary and high-pressure science for some decades[5–19], because ionic mobility affects thermal and electrical conductivity deep inside planets, and therefore their thermal evolution and ability to sustain magnetic fields. For example, it has been reported that the body centered cubic (bcc) phase of superionic ice transforms to a face centered cubic (fcc) phase, which is also superionic[11]; the latter has reportedly been seen in recent shock wave experiments[18,19] Sun et al.[14] reported a superionic state in close-packed and $P2_1/c$ phases of ice at higher pressures, and French et al. constructed thermodynamic potentials for the superionic bcc and fcc ice phases and calculated the phase boundary between them[15].

Superionicity of hydrogen in ammonia and ammonia compounds has also been studied[10,12,13,16,20,21]. Methane is also an important component of giant planets in addition to water and ammonia[17]. Superionic states have not been found in methane, due to the polymerization and release of hydrogen that occurs in methane at high pressures and temperatures[22–25]. Such polymerization may result in “diamond rain” in the icy planets.[26] In addition to the superionic states, the plastic phase in molecular crystals such as ammonia, in which protons rotate around the fixed nitrogen atoms, has been reported to emerge at certain pressure and temperature ranges[10]. The plastic phase and rotational motion in water have been studied under high pressure[27–29]. Very recently, Li et al.[30] found that colossal barocaloric effects in plastic crystals may have potential applications in solid-state refrigeration technologies.

While hydrogen-rich compounds have been studied extensively, this does not hold for helium-containing compounds. Traditionally helium is seen as the most inert element because of its closed-shell electronic configuration, but recently helium has been found to react under high pressure with metals[31,32] and ionic compounds[33–35]. Liu et al.[33] attributed the reactivity of helium with ionic compounds to the lowering of the Madelung energy between ions arising from the insertion of helium. At high pressures, helium has also been reported to form van der Waals (vdW) compounds with atoms such as neon[36] and covalent molecules such as ammonia[21], water[37–39], nitrogen[40–42], carbon dioxide[43] and arsenolite[44].

Superionicity involving helium has rarely been studied. Technically, helium is expected to diffuse as a neutral entity rather than an ionic entity, but a partially diffusive state involving helium has significant implications for thermal conductivities and viscosities. One such example is the helium-iron compound FeHe[32]. The superionic phase of FeHe occurs at pressures above 2 TPa and temperatures higher than 12,000 K. Several superionic phases have recently been found in helium-water mixtures, which show novel behaviors such as simultaneous superionicity of hydrogen and helium[39]. However, the possibility of compounds in the helium-methane system under high pressures and the nature of their high-temperature behavior are still open questions. This is despite these species forming significant portions of icy planetary atmospheres and mantles, respectively. Their miscibility is then relevant for the atmosphere-mantle boundary region, which is expected to feature large compositional gradients[45,46]. We have therefore investigated helium-methane mixtures at high pressures and temperatures.

RESULTS

In this work, searches for helium-methane compounds were performed using a machine learning accelerated crystal structure prediction method[47]. Structural optimizations, ab initio molecular dynamics (AIMD) simulations, enthalpies and electronic structures were calculated using the Vienna ab initio simulation (VASP)

code[48] with projector augmented-wave potentials and the Perdew-Burke-Ernzerhof exchange-correlation functional (PBE)[49]. Further details of the calculations are provided in the Supplemental Material.

Thermodynamic stabilities of the newly predicted compounds were estimated from their relative enthalpies of formation compared with those of polymorphs of carbon, hydrogen, and helium, and C-H compounds predicted in previous works[23,25,50–52]. Using an optB88-vdW functional[53,54] and hard pseudopotentials, we predicted that a new structure with a helium-methane stoichiometry of 3:1 is stable from 55 to 155 GPa (as shown in Fig. 1(a)) which is much wider than the stable pressure region of pure methane molecular crystals. Because methane decomposes above 100 GPa, here we showed a C-H-He phase diagram rather than a He-CH_4 phase diagram. The formation energy of the compound is about 32 meV/f.u. at 110 GPa (Fig. 1(b)). We have also computed the enthalpy-pressure relations using the PBE and PBE + D3 functionals[55], as shown in the Supplemental Material, all of the results confirmed that He_3CH_4 is energetically stable. He_3CH_4 is a molecular crystal with a hexagonal space group (SG) $P6_3mc$ composed of helium and methane molecules. As shown in Fig. 1(c-d), helium chains are inserted into the open channels formed by the methane molecules. The packing of methane molecules in He_3CH_4 is the same as in the experimental hexagonal closed packed (HCP) methane phase at low pressure[56], which is very different from the high-pressure phases of methane with orthorhombic space groups. Another compound, $HeCH_4$ with SG $P2_1/c$, is stable over a narrow range of pressures around 105 GPa. In addition, we have also found several metastable compounds, including $HeCH_4$ with SG $P2_1$, He2CH_4 with SG $P31m$ and $P2_1/m$, and $He_2(CH_4)_3$ with SG Cm. These metastable phases are very close to the convex hull. The phase diagrams under different pressures are shown in the Supplemental Material.

He_3CH_4 is an insulator with a large band gap of 8.9 eV at 50 GPa, as shown in Fig. S11 in the supplemental information, it is higher than that of pure methane molecular crystals. The phonon band structures of He_3CH_4 at 0 and 50 GPa shown in the Supplemental Material indicate the dynamical stability of this compound. $HeCH_4$ is also

found to be an insulator with a large band gap and is dynamically stable. The conditions in the upper mantle regions of icy planets reach tens to hundreds of GPa and thousands of K[45]. To obtain the dynamical properties of He_3CH_4 we performed AIMD simulations within the pressure range 50-200 GPa and the temperature range 500-3000 K. The averaged mean squared displacements (MSD) of hydrogen, helium, and carbon atoms were calculated to study phase transitions induced by temperature and pressure. According to the diffusive behavior of the different atoms, the states of He_3CH_4 can be divided into four types: the solid phase, a plastic CH_4 phase, a plastic CH_4 with diffusive He, and the fluid phase.

We used three representative trajectories to reveal the differences between the states by comparing their MSD and motions, as shown in Fig. 2. All of the simulations start from the relaxed configuration at 150 GPa, which are independent, but with different temperatures. At 1000 K, the atoms are restricted to their equilibrium positions, and exhibit small vibrations. As shown in Fig. 2(a), the MSD of the atoms are extremely small in the simulations, thus He_3CH_4 remains in the solid phase at this temperature.

When the temperature increases to 1900 K, the compound transforms to the plastic CH_4 phase. As shown in Fig. 2(b), the averaged MSD of H atoms increases rapidly in a short timescale, and stays about 2.0 $^{\circ}A^2$ afterwards. This is deemed to be a plastic phase when the methane molecules are free to rotate around the carbon atoms with small fluctuations of C-H bond lengths and angles (Fig. 2(e)). Plastic phases have also been reported in pure methane[57], ice[27,58] and ammonia[10,12]. Meanwhile, the averaged MSD values of He and C atoms are still very small. Using the rigid molecule approximation[57] we have been able to calculate the theoretical MSD of the H atoms. Suppose that the methane molecules are rigid with fixed radius r_{CH}(the length of a C-H bond). For one of the H atoms, its initial position is $\boldsymbol{r}_0(r_{CH}, 0,0)$ in spherical coordinates. Since methane molecules rotate freely, the position of the H atom $\boldsymbol{r}(r_{CH}, \theta, \phi)$ is distributed uniformly over the sphere of radius r_{CH}.Therefore, the analytical MSD is:

$$\langle(\boldsymbol{r}-\boldsymbol{r}_0)^2\rangle = \frac{1}{4\pi}\int_0^{\pi} d\theta \int_0^{2\pi} d\phi \sin\theta\,(\boldsymbol{r}-\boldsymbol{r}_0^2) = \frac{2r_{CH}^2}{4\pi}\int_0^{\pi} d\theta \int_0^{2\pi} d\phi \sin\theta\,(1-\cos\theta) = 2r_{CH}^2 (1)$$

For the plastic CH_4 phase, the resulting MSD is $\langle(\boldsymbol{r}-\boldsymbol{r}_0)^2\rangle = 2.142\text{Å}^2$, which is very close to the value from our AIMD calculations ($2.169^{\circ}A^2$).

At higher temperatures (2350 K) methane molecules rotate while helium atoms are diffusive (Fig. 2(c)(f)), which leads to the formation of a superionic-like He state in He_3CH_4. The diffusion coefficient of helium atoms D_{He} is $4.81 \times 10^{-10} m^2/s$ from the velocity auto-correlation functions (VACFs). We obtain very similar results D_{He} =4.48 $\times 10^{-10} m^2/s$ from the MSD. Diffusion coefficients of helium along different directions were also calculated: $D_{He}^x = 3.79 \times 10^{-10} m^2/s$, $D_{He}^y = 4.02 \times 10^{-10} m^2/s$, $D_{He}^z = 6.62 \times 10^{-10} m^2/s$. The existence of open channels along the z axis in He_3CH_4 (Fig. 1(d)) can explain the anisotropy of diffusion coefficients. Heating the superionic phases of He_3CH_4 eventually leads to melting of the methane sublattice, which gives rise to the fluid phase.

We can further understand the dynamical processes of the He_3CH_4 structure at different temperatures by using the radial distribution function (RDF). C-H and C-He partial RDFs are shown in Fig. 3(a)(b) and others are shown in the Supplemental Material. The C-He, He-He, and H-He partial RDFs of the partially diffusive phase (2350 K, green lines) are very similar to those of the plastic phase (1900 K, red lines), but are clearly different from those of the fluid phase (2700 K, blue lines). We analyzed some trajectories of the partially diffusive phase and found that the diffusion of helium atoms maintains the order of the helium chains. In some cases of the partially diffusive phase we can see the plateaus in the averaged MSD of He. The performance of the diffusive helium atoms is similar to collective diffusion of ions in lithium battery cathode materials[59,60]. The atoms jump along the chains or hop from one chain to another and therefore the RDFs remain solid-like. However, in the fluid phase, the sublattices of helium and methane have already melted and the RDFs are liquid-like. Finally, the first peak of the C-H RDFs remains essentially unchanged deep into the fluid phase. This indicates that the integrity of the methane molecules is maintained up to the highest temperature.

The superionic state in helium-methane differs from the few other examples of superionic helium[32,39] because plastic CH_4 and diffusive He states coexist. Plastic and superionic phases also appear in the phase diagram of ammonia and ice[10,12,58], but they cannot coexist since both the plastic and diffusive atoms in ammonia and water are protons.

From the results of the extensive AIMD simulations, we proposed a phase diagram of He_3CH_4 between 50 and 200 GPa and below 3000 K (Fig. 4). The colored dots represent independent NVT simulations which are classified by their averaged MSDs and RDFs (tests with the NPT ensemble confirm these classifications, see the SM). The phase boundaries divide the diagram into four regions: solid, plastic CH_4, plastic CH_4 + diffusive He and fluid phases. The partially diffusive phase appears at pressures above 70 GPa within a narrow range. Compared with helium-water compounds, He_3CH_4 is dominated by dispersion interactions between methane molecules, which are much weaker than the hydrogen bonds between water molecules. Therefore the ice frameworks in helium-water compounds are more stable than the sublattice of methane molecules. There are many open channels in helium-water compounds, which results in a much wider partially diffusive region in helium-water than that in the helium-methane system. To validate the superionicity of helium we have performed AIMD calculations at 150 GPa using hard pseudopotentials. The results are shown in the Supplemental Material and the appearance of the partially diffusive phase at high temperatures is unaffected.

To investigate the interactions in He_3CH_4 we have applied a real-space analysis to the helium-methane compound. According to the electron localization function (ELF) shown in Fig. 3(d), strong intramolecular covalent bonds persist between carbon and hydrogen atoms while the interactions between methane and helium molecules are of closed-shell character. The types of intermolecular interactions in He_3CH_4 can be determined using the atoms-in-molecules (AIM) theory[61] and reduced density gradient (RDG) analysis[62]. Based on AIM, a topological analysis of the electron density $\rho(\mathbf{r})$ was carried out to compute atomic Bader charges and search for bond critical points (BCPs).

We found that the charge transfer in He_3CH_4 is less than $0.03e^-$ between carbon and hydrogen. This is consistent with the fact that the electronegativities of carbon and hydrogen are similar and methane cannot participate in hydrogen bonding. A BCP connecting a pair of atoms provides important information about the bonding between atoms. We show all of the non-equivalent BCPs and their properties in the Supplemental Material. The first and second BCPs represent the bonds inside methane molecules. The electron densities at these BCPs are much larger than others and the negative Laplacian values indicate the concentration of electrons between the carbon and hydrogen atoms. These are typical features of covalent bonding. Other BCPs with small densities and positive Laplacian values are characteristic of dispersion interactions. Furthermore, reduce density gradient analysis has been applied to the electron density. As shown in Fig. 3(c), the spikes at low density, the low-gradient region (inside the red dashed box) reflects the existence of non-covalent interactions[62] in He_3CH_4. The distinct spikes are very near zero, indicating that the type is vdW interactions, which are weaker than hydrogen bonds in helium-water[39] and helium-ammonia compounds[21].

DISCUSSION

The isotopic effects in hydrogen are important in some cases[63] and we have accounted for them in the helium methane compound by comparing the vibrational densities of states (VDOS) of He_3CH_4 and He_3CD_4 (Supplemental Material). Within the harmonic approximation, isotopic effects lead to changes in the atomic mass and a decrease in the phonon frequencies. The frequency of the highest peak in the partial VDOS drops from about 3700 cm^{-1} for hydrogen to about 2700 cm^{-1} for deuterium, with a ratio of about $1/\sqrt{2}$. Since strong covalent bonds exist between carbon and hydrogen/deuterium, the highest phonon peaks of carbon have the same tendencies as the isotopic effects. In contrast, the frequency region of the helium VDOS does not change substantially, because the vdW interactions between helium and methane are weak. The isotopic effects can also influence dynamical properties, and therefore we conducted AIMD calculations for He_3CD_4 at 2350 K and compared the VDOS of

He_3CH_4 and He_3CD_4 at high temperatures. For carbon and hydrogen/deuterium the reduction of the frequencies also appears with the ratio of $1/\sqrt{2}$. For helium, the partial VDOS is very similar. This demonstrates that isotopic effects do not substantially affect the superionicity of the helium-methane compound.

In previous studies nuclear quantum effects were considered for ice[15] and mixtures of methane, ammonia, and water[64]. The nuclear quantum corrections for He_3CH_4 at different densities and temperatures are shown in the Supplemental Material. The quantum corrections for the helium-methane compounds are slightly larger than those for ice[15] because of the higher proportion of hydrogen in the compound and the lower temperature region in our simulations.

CONCLUSIONS

In summary, we have predicted a helium-methane compound (He_3CH_4) that is stable at pressures relevant to upper mantle conditions of icy planets. The inclusion of He atoms highly changes the packing of methane molecules and the stable pressure region of the helium-methane compound is much wider than that of pure methane. He insertion also changes the electronic properties of methane. For example, the band gap of He_3CH_4 is larger than that of pure methane. Moreover, the phase diagram of He_3CH_4 has been investigated and a novel phase of coexistence of plastic methane and diffusive helium has been found. The temperature range of the partially diffusive regime in helium-methane is narrower than that in the helium-water system, due to the weaker interactions between the methane molecules, which results in a relatively fragile framework and an easier transition to the fluid state than in the helium-water system. In addition, we observed anisotropy in the He diffusion, which is related to the structure of the compound. We have also analyzed the interactions in He_3CH_4 and their effects on the phase diagram in comparison with previously predicted helium-water compounds. This work should be helpful in constructing models of icy giant planets, and it would be very instructive to investigate how much the finite-temperature miscibility of helium and methane reflects our ground state results[65].

METHODS

We used a Bayesian Optimization based crystal structure prediction method[45] combined with VASP to predict new compounds for the He-CH_4 system. The prediction results have been checked by ab initio random structure searching (AIRSS)[66].The optB88-vdW functional[53] was employed to account for vdW interactions in the calculations of enthalpies and electronic structures. A basis set energy cutoff of 720 eV was used except for the AIMD calculations, for which a lower cutoff energy of 625 eV was used for reducing the computational cost of extensive AIMD simulations. The Brillouin zone was sampled with a Monkhorst-Pack k-point mesh with a spacing of $2\pi \times 0.03$ Å^{-1}. The phonon dispersion curves were calculated using $2 \times 2 \times 2$ supercells with PHONOPY code[67] to validate the dynamical stabilities of the predicted structures. The atoms-in-molecules (AIM)[61] and reduce density gradient (RDG)[62] analysis of the electron density $\rho(r)$ was performed using the critic2 code[68]. We used orthorhombic supercells containing 256 atoms to perform AIMD simulations for He_3CH_4 in the NVT ensemble with Γ-centered k-points sampling. The time step of AIMD was set to 1 fs and all simulations were carried out with at least 3000 steps. Some trajectories were extended to more than 10 ps to confirm the stabilities. In addition, to validate our results we employed hard pseudopotentials for hydrogen and carbon and repeated the calculations. The cutoff energy of 1000 eV was used to calculate pressure-composition phase diagrams. A cutoff energy of 910 eV was used for the AIMD simulations. The nuclear quantum corrections of free energies are calculated from the AIMD trajectories using the method proposed in Ref[15].

ACKNOWLEDGMENTS

J.S. gratefully acknowledges financial support from the National Key R&D Program of China (Grant No. 2016YFA0300404), the National Natural Science Foundation of China (Grant Nos. 11974162 and 11834006), the Fundamental Research Funds for the Central Universities. C.J.P. and R.J.N. acknowledge financial support from the Engineering and Physical Sciences Research Council

(EPSRC) of the U.K. under grants [EP/G007489/2] (C.J.P.) and [EP/P034616/1] (R.J.N.). C.J.P. also acknowledges financial support from EPSRC and the Royal Society through a Royal Society Wolfson Research Merit award. The calculations were carried out using supercomputers at the High Performance Computing Center of Collaborative Innovation Center of Advanced Microstructures, high performance supercomputing center of Nanjing University, "Tianhe-2" at NSCC-Guangzhou and the CSD3 Peta4 CPU/KNL machine in the University of Cambridge.

AUTHOR CONTRIBUTIONS

J.S. conceived and led the project. H.G. and C.J.P performed the calculations. J.S, H.G. and C.L. made the analysis. J.S., H.G., A.H., and R.J.N wrote the manuscript. All authors discussed the results and commented on the manuscript.

The authors declare no competing interests.

REFERENCES

1. Stevenson, D. J. Metallic helium in massive planets. *Proc. Natl. Acad. Sci.* **105**, 11035–11036 (2008).
2. Ryzhkin, I. A. Superionic transition in ice. *Solid State Communications* **56**, 57–60 (1985).
3. Demontis, P., LeSar, R. & Klein, M. L. New High-Pressure Phases of Ice. *Phys. Rev. Lett.* **60**, 2284–2287 (1988).
4. Cavazzoni, C., Chiarotti, G. L., Scandolo, S., *et al.* Superionic and Metallic States of Water and Ammonia at Giant Planet Conditions. *Science* **283**, 44–46 (1999).
5. Yakushev, V. V., Postnov, V. I., Fortov, V. E., *et al.* Electrical conductivity of water during quasi-isentropic compression to 130 GPa. *J. Exp. Theor. Phys.* **90**, 617–622 (2000).

6. Chau, R., Mitchell, A. C., Minich, R. W., *et al.* Electrical conductivity of water compressed dynamically to pressures of 70–180 GPa (0.7–1.8 Mbar). *J. Chem. Phys.* **114**, 1361–1365 (2001).
7. Goncharov, A. F., Goldman, N., Fried, L. E., *et al.* Dynamic Ionization of Water under Extreme Conditions. *Phys. Rev. Lett.* **94**, 125508 (2005).
8. French, M., Mattsson, T. R., Nettelmann, N., *et al.* Equation of state and phase diagram of water at ultrahigh pressures as in planetary interiors. *Phys. Rev. B* **79**, 054107 (2009).
9. Redmer, R., Mattsson, T. R., Nettelmann, N., *et al.* The phase diagram of water and the magnetic fields of Uranus and Neptune. *Icarus* **211**, 798–803 (2011).
10. Ninet, S., Datchi, F. & Saitta, A. M. Proton Disorder and Superionicity in Hot Dense Ammonia Ice. *Phys. Rev. Lett.* **108**, 165702 (2012).
11. Wilson, H. F., Wong, M. L. & Militzer, B. Superionic to Superionic Phase Change in Water: Consequences for the Interiors of Uranus and Neptune. *Phys. Rev. Lett.* **110**, 151102 (2013).
12. Bethkenhagen, M., French, M. & Redmer, R. Equation of state and phase diagram of ammonia at high pressures from ab initio simulations. *J. Chem. Phys.* **138**, 234504 (2013).
13. Bethkenhagen, M., Cebulla, D., Redmer, R., *et al.* Superionic Phases of the 1:1 Water–Ammonia Mixture. *J. Phys. Chem. A* **119**, 10582–10588 (2015).
14. Sun, J., Clark, B. K., Torquato, S., *et al.* The phase diagram of high-pressure superionic ice. *Nat. Commun.* **6**, 8156 (2015).

15. French, M., Desjarlais, M. P. & Redmer, R. *Ab initio* calculation of thermodynamic potentials and entropies for superionic water. *Phys. Rev. E* **93**, 022140 (2016).
16. Jiang, X., Wu, X., Zheng, Z., *et al.* Ionic and superionic phases in ammonia dihydrate NH3 H2O under high pressure. *Phys. Rev. B* **95**, 144104 (2017).
17. Bethkenhagen, M., Meyer, E. R., Hamel, S., *et al.* Planetary Ices and the Linear Mixing Approximation. *ApJ* **848**, 67 (2017).
18. Millot, M., Hamel, S., Rygg, J. R., *et al.* Experimental evidence for superionic water ice using shock compression. *Nature Physics* **14**, 297 (2018).
19. Millot, M., Coppari, F., Rygg, J. R., *et al.* Nanosecond X-ray diffraction of shock-compressed superionic water ice. *Nature* **569**, 251 (2019).
20. Song, X., Yin, K., Wang, Y., *et al.* Exotic Hydrogen Bonding in Compressed Ammonia Hydrides. *J. Phys. Chem. Lett.* **10**, 2761–2766 (2019).
21. Liu, C., Gao, H., Hermann, A., *et al.* Plastic and superionic helium ammonia compounds under high pressure and high temperature. *Physical Review X* (2020). (in press)
22. Hirai, H., Konagai, K., Kawamura, T., *et al.* Polymerization and diamond formation from melting methane and their implications in ice layer of giant planets. *Phys. Earth. Planet. Inter.* **174**, 242–246 (2009).
23. Gao, G., Oganov, A. R., Ma, Y., *et al.* Dissociation of methane under high pressure. *J. Chem. Phys.* **133**, 144508 (2010).
24. Sherman, B. L., Wilson, H. F., Weeraratne, D., *et al.* Ab initio simulations of hot dense methane during shock experiments. *Phys. Rev. B* **86**, 224113 (2012).

25. Conway, L. J. & Hermann, A. High Pressure Hydrocarbons Revisited: From van der Waals Compounds to Diamond. *Geosciences* **9**, 227 (2019).
26. Kraus, D., Vorberger, J., Pak, A., *et al.* Formation of diamonds in laser-compressed hydrocarbons at planetary interior conditions. *Nature Astronomy* **1**, 606 (2017).
27. Takii, Y., Koga, K. & Tanaka, H. A plastic phase of water from computer simulation. *J. Chem. Phys.* **128**, 204501 (2008).
28. Aragones, J. L. & Vega, C. Plastic crystal phases of simple water models. *J. Chem. Phys.* **130**, 244504 (2009).
29. Bove, L. E., Klotz, S., Strässle, Th., *et al.* Translational and Rotational Diffusion in Water in the Gigapascal Range. *Phys. Rev. Lett.* **111**, 185901 (2013).
30. Li, B., Kawakita, Y., Ohira-Kawamura, S., *et al.* Colossal barocaloric effects in plastic crystals. *Nature* **567**, 506 (2019).
31. Dong, X., Oganov, A. R., Goncharov, A. F., *et al.* A stable compound of helium and sodium at high pressure. *Nat. Chem.* **9**, 440–445 (2017).
32. Monserrat, B., Martinez-Canales, M., Needs, R. J., *et al.* Helium-Iron Compounds at Terapascal Pressures. *Phys. Rev. Lett.* **121**, 015301 (2018).
33. Liu, Z., Botana, J., Hermann, A., *et al.* Reactivity of He with ionic compounds under high pressure. *Nat. Commun.* **9**, 951 (2018).
34. Zhang, J., Lv, J., Li, H., *et al.* Rare Helium-Bearing Compound ${\mathrm{FeO}}_{2}\mathrm{He}$ Stabilized at Deep-Earth Conditions. *Phys. Rev. Lett.* **121**, 255703 (2018).

35. Gao, H., Sun, J., Pickard, C. J., *et al.* Prediction of pressure-induced stabilization of noble-gas-atom compounds with alkali oxides and alkali sulfides. *Phys. Rev. Materials* **3**, 015002 (2019).

36. Loubeyre, P., Jean-Louis, M., LeToullec, R., *et al.* High pressure measurements of the He-Ne binary phase diagram at 296 K: Evidence for the stability of a stoichiometric Ne(He${)}_{2}$ solid. *Phys. Rev. Lett.* **70**, 178–181 (1993).

37. Liu, H., Yao, Y. & Klug, D. D. Stable structures of He and ${\mathrm{H}}_{2}\mathrm{O}$ at high pressure. *Phys. Rev. B* **91**, 014102 (2015).

38. Teeratchanan, P. & Hermann, A. Computational phase diagrams of noble gas hydrates under pressure. *J. Chem. Phys.* **143**, 154507 (2015).

39. Liu, C., Gao, H., Wang, Y., *et al.* Multiple superionic states in helium–water compounds. *Nat. Phys.* **15**, 1065–1070 (2019).

40. Vos, W. L., Finger, L. W., Hemley, R. J., *et al.* A high-pressure van der Waals compound in solid nitrogen-helium mixtures. *Nature* **358**, 46–48 (1992).

41. Ninet, S., Weck, G., Loubeyre, P., *et al.* Structural and vibrational properties of the van der Waals compound (N${}_{2}$)${}_{11}$He up to 135 GPa. *Phys. Rev. B* **83**, 134107 (2011).

42. Li, Y., Feng, X., Liu, H., *et al.* Route to high-energy density polymeric nitrogen t -N via He−N compounds. *Nat. Commun.* **9**, 722 (2018).

43. Li, D., Liu, Y., Tian, F., *et al.* High-pressure structures of helium and carbon dioxide from first-principles calculations. *Solid State Commun.* **283**, 9–13 (2018).

44. Sans, J. A., Manjón, F. J., Popescu, C., *et al.* Ordered helium trapping and bonding in compressed arsenolite: Synthesis of As4O6 2He. *Phys. Rev. B* **93**, 054102 (2016).

45. Nettelmann, N., Wang, K., Fortney, J. J., *et al.* Uranus evolution models with simple thermal boundary layers. *Icarus* **275**, 107–116 (2016).

46. French, M. & Nettelmann, N. Viscosity and Prandtl Number of Warm Dense Water as in Ice Giant Planets. *ApJ* **881**, 81 (2019).

47. Xia, K., Gao, H., Liu, C., *et al.* A novel superhard tungsten nitride predicted by machine-learning accelerated crystal structure search. *Sci. Bull.* **63**, 817–824 (2018).

48. Kresse, G. & Furthmüller, J. Efficient iterative schemes for \textit{ab initio} total-energy calculations using a plane-wave basis set. *Phys. Rev. B* **54**, 11169–11186 (1996).

49. Perdew, J. P., Burke, K. & Ernzerhof, M. Generalized Gradient Approximation Made Simple. *Phys. Rev. Lett.* **77**, 3865–3868 (1996).

50. Wen, X.-D., Hand, L., Labet, V., *et al.* Graphane sheets and crystals under pressure. *PNAS* **108**, 6833–6837 (2011).

51. Liu, Y., Duan, D., Tian, F., *et al.* Crystal structures and properties of the CH4H2 compound under high pressure. *RSC Adv.* **4**, 37569–37574 (2014).

52. Saleh, G. & Oganov, A. R. Novel Stable Compounds in the C-H-O Ternary System at High Pressure. *Sci. Rep.* **6**, 32486 (2016).

53. Klimeš, J., Bowler, D. R. & Michaelides, A. Chemical accuracy for the van der Waals density functional. *J. Phys.: Condens. Matter* **22**, 022201 (2010).

54. Dion, M., Rydberg, H., Schröder, E., *et al.* Van der Waals Density Functional for General Geometries. *Physical Review Letters* **92**, (2004).

55. Grimme, S., Antony, J., Ehrlich, S., *et al.* A consistent and accurate ab initio parametrization of density functional dispersion correction (DFT-D) for the 94 elements H-Pu. *The Journal of Chemical Physics* **132**, 154104 (2010).

56. Bini, R. & Pratesi, G. High-pressure infrared study of solid methane: Phase diagram up to 30 GPa. *Phys. Rev. B* **55**, 14800–14809 (1997).

57. Spanu, L., Donadio, D., Hohl, D., *et al.* Theoretical investigation of methane under pressure. *J. Chem. Phys.* **130**, 164520 (2009).

58. Hernandez, J.-A. & Caracas, R. Proton dynamics and the phase diagram of dense water ice. *J. Chem. Phys.* **148**, 214501 (2018).

59. He, X., Zhu, Y. & Mo, Y. Origin of fast ion diffusion in super-ionic conductors. *Nat Commun* **8**, 15893 (2017).

60. Zimmermann, N. E. R., Hannah, D. C., Rong, Z., *et al.* Electrostatic Estimation of Intercalant Jump-Diffusion Barriers Using Finite-Size Ion Models. *J. Phys. Chem. Lett.* **9**, 628–634 (2018).

61. Bader, R. F. W. A quantum theory of molecular structure and its applications. *Chem. Rev.* **91**, 893–928 (1991).

62. Johnson, E. R., Keinan, S., Mori-Sánchez, P., *et al.* Revealing Noncovalent Interactions. *J. Am. Chem. Soc.* **132**, 6498–6506 (2010).

63. Hermann, A., Ashcroft, N. W. & Hoffmann, R. Isotopic differentiation and sublattice melting in dense dynamic ice. *Phys. Rev. B* **88**, 214113 (2013).

64. Meyer, E. R., Ticknor, C., Bethkenhagen, M., *et al.* Bonding and structure in dense multi-component molecular mixtures. *J. Chem. Phys.* **143**, 164513 (2015).

65. Schöttler, M. & Redmer, R. Ab Initio Calculation of the Miscibility Diagram for Hydrogen-Helium Mixtures. *Phys. Rev. Lett.* **120**, 115703 (2018).

66. Pickard, C. J. & Needs, R. J. *Ab initio* random structure searching. *Journal of Physics: Condensed Matter* **23**, 053201 (2011).

67. Togo, A. & Tanaka, I. First principles phonon calculations in materials science. *Scr. Mater.* **108**, 1–5 (2015).

68. Otero-de-la-Roza, A., Johnson, E. R. & Luaña, V. Critic2: A program for real-space analysis of quantum chemical interactions in solids. *Comp. Phys. Commun.* **185**, 1007–1018 (2014).

Additional information

Supplementary information is available for this paper at https://xxx.xxx-xxx

Figures

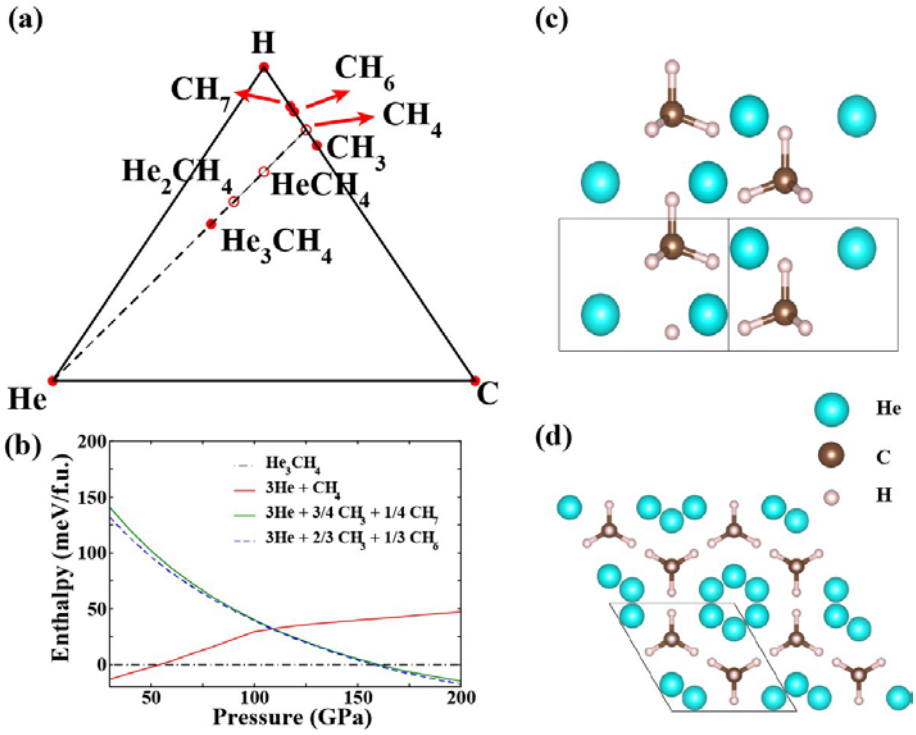

FIG. 1. Energetic stability and crystal structures of He-CH4 compound. (a) C-H-He phase diagram at 155 GPa, (b) enthalpy-pressure relations for the C-H-He compounds and the crystal structure of He_3CH_4 viewed along [110] (c) and [001](d). The solid and open circles represent stable and metastable phases, respectively.

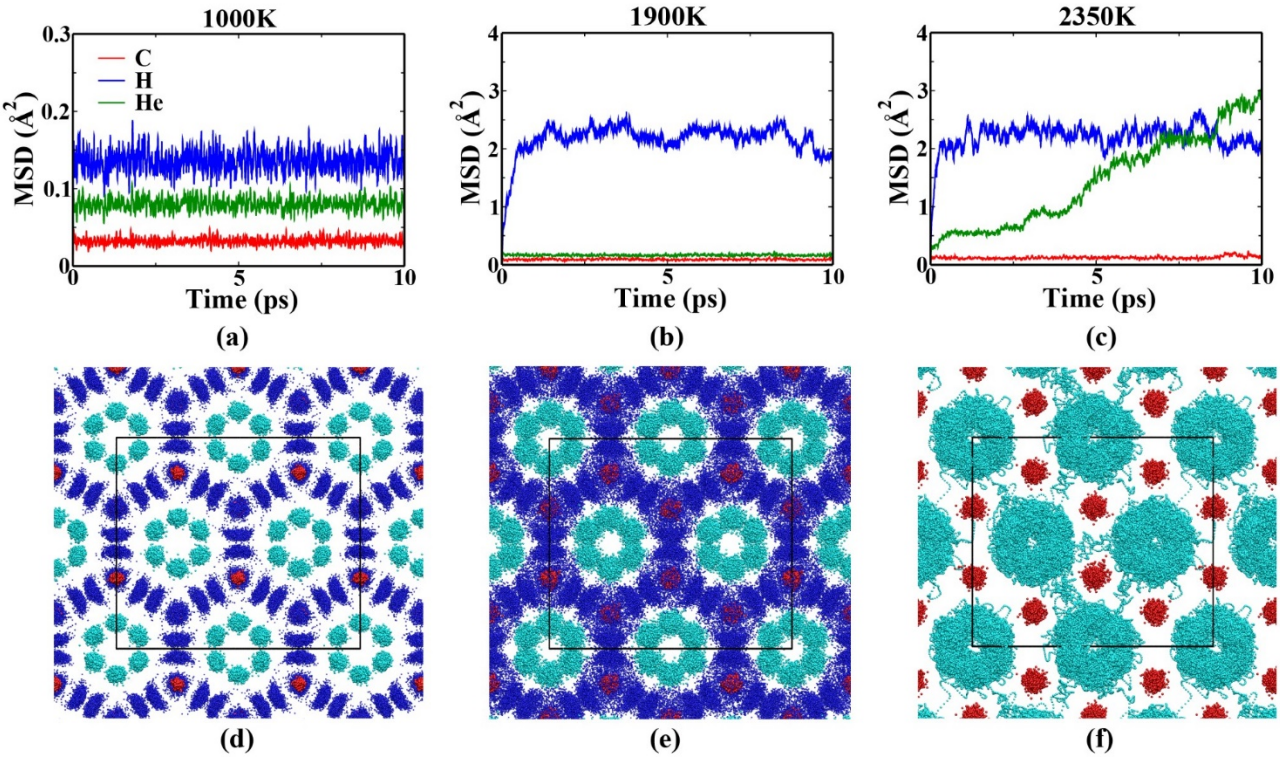

FIG. 2. Dynamical behaviors of He_3CH_4 at high pressure from AIMD simulations at 1000 K, 1900 K and 2350 K. (a-c) The averaged MSD of H, He and C atoms at different temperatures. (d-f) Representations of trajectories at different temperatures in the last 10 ps. Blue, cyan and red dots represent H, He and C atoms, respectively. At 2350 K, the trajectories of H and He atoms overlap with one another, and therefore we only show He trajectories here.

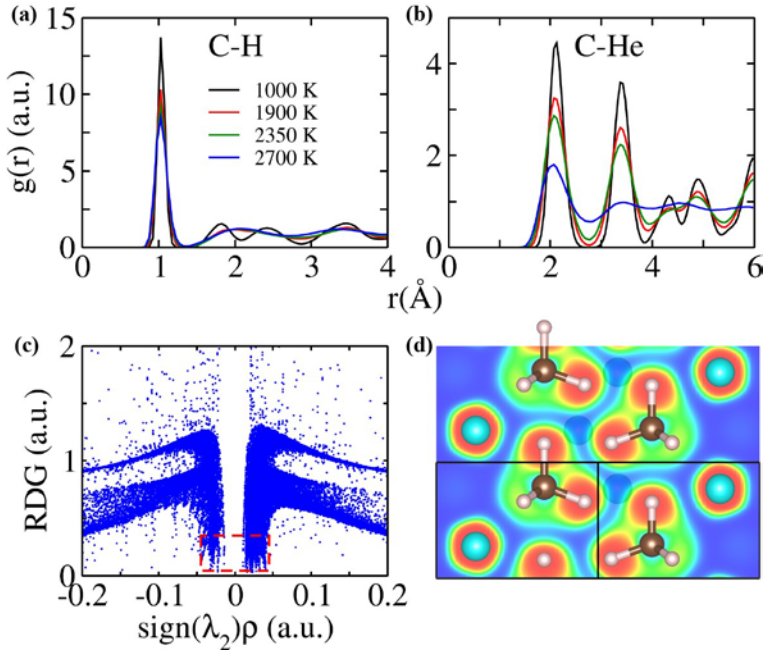

FIG. 3. Dynamical structure and interaction analysis. Radial distribution functions (RDFs) for C-H (a) and C-He (b) pairs in He_3CH_4 at around 150 GPa and heating to about 1000 K (solid phase), 1900 K (plastic phase), 2350 K (coexistence of plastic and partially diffusive phase) and 2700 K (fluid phase). (c) Plots of the reduce density gradient (RDG) versus the electron density multiplied by the sign of the second largest eigenvalue of the electron-density Hessian matrix. (d) ELF plotted in the (110) plane.

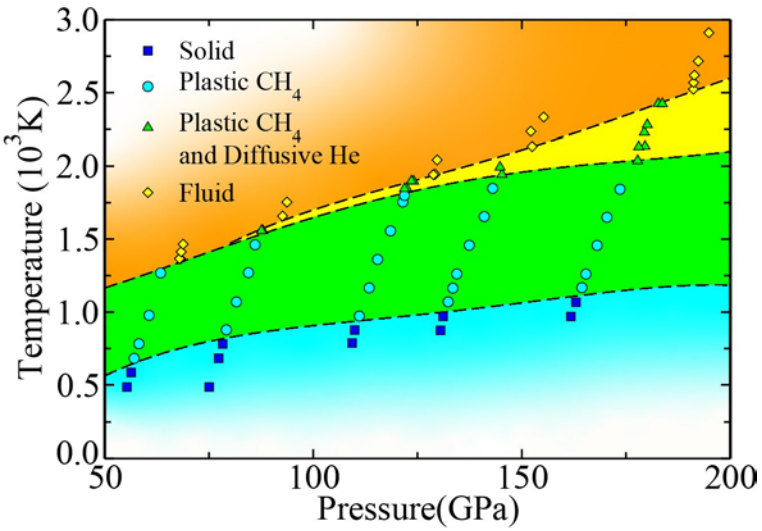

FIG. 4. Phase diagram of He_3CH_4 as determined in this work. Each symbol represents an AIMD simulation. The dashed lines are phase boundaries.